# Breakups of Chitosan microcapsules in extensional flow

Revaz Chachanidze, Kaili Xie, Jinming Lyu, Marc Jaeger, Marc Leonetti

# Graphical Abstract

## Breakups of Chitosan Microcapsules in Extensional Flow

Revaz Chachanidze, Kaili Xie,Jinming Lyu,Marc Jaeger,Marc Leonetti

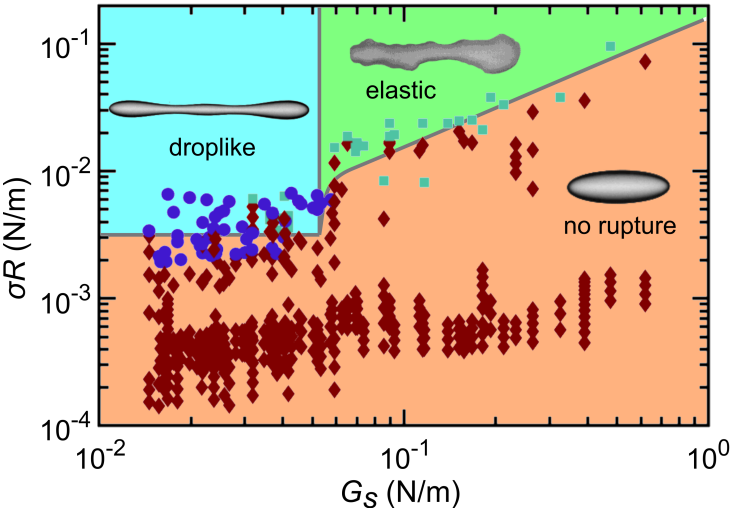

# Highlights

## Breakups of Chitosan Microcapsules in Extensional Flow

Revaz Chachanidze, Kaili Xie,Jinming Lyu,Marc Jaeger,Marc Leonetti

- Weakly cohesive Chitosan microcapsules were deformed up to breakup in an extensional flow with orthogonal observations.
- Two mechanisms of rupture regimes of microcapsules were revealed: fluid-like and solid-like behaviours.
- The dual response of microcapsule rupture in flow is closely correlated to the shell structure.

# Breakups of Chitosan Microcapsules in Extensional Flow

Revaz Chachanidze[d,1], Kaili Xie[b,c,d,1], Jinming Lyu[b], Marc Jaeger[b] and Marc Leonetti[a,c,d,*]

[a]Aix Marseille Univ, CNRS, CINaM, Marseille, France
[b]Aix Marseille Univ, CNRS, Centrale Marseille, M2P2, Marseille, France
[c]Aix Marseille Univ, CNRS, Centrale Marseille, IRPHE, Marseille, France
[d]Univ. Grenoble Alpes, CNRS, Grenoble INP, LRP, Grenoble, France

ARTICLE INFO

*Keywords*:
microcapsule
breakup
breakage
extensional flow
fluid/solid behaviors
surface rheology
fragmentation

ABSTRACT

The controlled rupture of a core-shell capsule and the timely release of encapsulated materials are essential steps of the efficient design of such carriers. The mechanical and physico-chemical properties of their shells (or membranes) mainly govern the evolution of such systems under stress and notably the link between the dynamics of rupture and the mechanical properties. This issue is addressed considering weakly cohesive shells made by the interfacial complexation of Chitosan and PFacid in a planar extensional flow. Three regimes are observed, thanks to the two observational planes. Whatever the time of reaction in membrane assembly, there is no rupture in deformation as long as the hydrodynamic stress is below a critical value. At low times of complexation (weak shear elastic modulus), the rupture is reminiscent of the breakup of droplets: a dumbell or a waist. Fluorescent labelling of the membrane shows that this process is governed by continuous thinning of the membrane up to the destabilization. It is likely that the membrane shows a transition from a solid to liquid state. At longer times of complexation, the rupture has a feature of solid-like breakup (breakage) with a discontinuity of the membrane. The maximal internal constraint determined numerically marks the initial location of breakup as shown. The pattern becomes more complex as the elongation rate increases with several points of rupture. A phase diagram in the space parameters of the shear elastic modulus and the hydrodynamic stress is established.

## 1. Introduction

Dispersed multiphase flows containing immiscible droplets occur frequently in nature [1] as well as in industrial processes [2, 3]. Artificially, to stabilize the multiphase systems, surfactants [4], lipids and copolymers [5, 6], proteins [7], nanoparticles [8–10] or thin membranes [11, 12] are often embedded on the liquid-air or liquid-liquid interfaces. Such surface agents modify the properties of the droplet interface allowing for the additional functionality and tailored mechanical behaviours [13, 14]. Artificial microcapsules are striking examples of such complex systems, generally consisting of liquid drops enclosed by thin shells, also called membrane and are widely attractive in food [15, 16], cosmetics [17] and biomedicine [18] applications for the controlled release of encapsulated substances [19].

Recent advances in microcapsules focus on the development of smart system related to the precise delivery and release of active agents [20, 21]. External stimuli, such as environmental pH [22, 23], temperature [24], light [25] and stress [26, 27] are proven to be effective strategies for controlled release rate and targeted delivery of the encapsulated materials. In designing functional microcapsules for specific purposes, understanding and controlling redthe shell properties, including shell structure, permeability and mechanical properties, are crucial and fundamental. The mechanical aspect is obviously important for mechanical stability issues, particularly in the control of stress-responsive burst release. Knowing the conditions of microcapsule breakup is required for capsule design if the rapid release of the content is desired via breakup. The shells are typically composed of polymers [28–30] with electrostatic adsorption [11, 31] leading to weak cohesion and viscoplastic behavior [11, 32] or with cross-linking [33, 34] for example. The cross-linked membranes can also lead to capsules which can sustain extension more than 200 % without visible failure [35], a rubber-like behavior. In this paper, we only consider the rupture of weakly cohesive

*Corresponding author: marc.leonetti@cnrs.fr
ORCID(s): 0000-0001-7511-2910 (R. Chachanidze); 0000-0001-5465-4067 (.K. Xie); 0000-0001-7511-2910 (M. Jaeger)
[1]These authors contribute equally.

microcapsules which sustain from moderate to large extensions before breaking. The capsule membrane is assembled via interfacial complexation using chitosan and phosphatidic fatty acids (referred to as PFacid). We study the rupture of Chitosan/PFacid capsules which are ductile and manifest important plasticity [11].

Regarding this, to our knowledge the earliest experimental work on breakup of synthetic capsules was performed by Chang and Olbricht [36]. Millimetric nylon capsules were subjected to a counter-rotating Couette flow; the breakup occurred near the tip of the major axis of deformed capsules where tears were observed. Maximum extension associated with the thinning of the shell due to flow-induced deformation was suggested as the driving force for breakup. A similar phenomenon of tip-induced tears was observed much clearly with polysiloxane capsules at low density of polymers [32] and with inflated and noninflated human serum albumin (HSA) capsules [37]. In the last report, tears appear after several cycles of tank-treading suggesting a possible fatigue failure. At higher elastic capillary number, the HSA capsule breaks in the middle like a droplet close to the threshold. This is reminiscent of the results observed for the breakup of surfactant-laden drops [38]. At higher density of polysiloxane, a local breakup (failure) is potentially observed close to the center (the axis of vorticity) looking like a small straight line along the stretching direction [32]. Following tank-treading, this damaged domain rotates and experiences a temporal variation of stresses. It is challenging to characterize the conditions of this domain emergence and to determine how it evolves and its consequences on the capsule. Note that this behavior was not observed by Chang and Olbricht [36].

Finally, these studies highlight two key elements. First, the nonlinear surface rheology plays an essential role in capsule breakup. Indeed, some membranes of microcapsules may undergo complicated behaviours, for example solid-like to liquid-like transition [39]. Second, the coupling of rotation and elongation in the shear flow leads to an additional complexity in capsule breakup process.

Differently to shear flow, microcapsules exposed to extensional flow [11, 34] do not exhibit complex dynamics [40–42], which allows us to understand the mechanism of breakup in a simpler way. In the extensional flow, an initially spherical microcapsule is observed being stretched in the extensional direction and compressed in the perpendicular direction by the hydrodynamic stress; a pancake-like shape occurs [35]. At steady state, the hydrodynamic stress is balanced by the shell deformation which remains motionless. The internal liquid thus also remains motionless; viscosity ratios (internal to external liquids) do not play a crucial role contrary to the case of droplets [38]. This type of load offers a promising strategy for studying microcapsule breakup process. Indeed, this flow configuration has been previously applied to droplets and viscoelastic flows [43–45].

In this work, we experimentally investigate the breakup of microcapsules with well-controlled and tunable shell rheological properties in a planar extensional flow. The objective is to understand the breakup mechanism of microcapsule submerged in another viscous fluid and the correlation with the shell rheological properties. Individual microcapsules are deformed several times with incremental extensional rate up to the point of breakage. Multi-directional visualizations are employed showing new insights on capsule breakup in deformation. Two fundamentally different regimes of breakup are reported. The constructed phase diagram of breakup reveals the qualitative transition from liquid-like to solid-like behaviors in capsule shell.

## 2. Materials and methods

### 2.1. Materials

Chitosan powder with medium molecular weight and 75-85% deacetylation was purchased from Sigma-Aldrich. Anionic surfactant, phosphatidic fatty acids (referred to as PFacid, food grade E442) was obtained from Palsgaard. Glycerol (> 99% of purity), hydrochloric acid (1 mol/L) and sodium hydroxide (1 mol/L) were purchased from VWR. The fluorescent dye, Hostasol Yellow 3G (HY-3G), was acquired from Clariant. Rapeseed oil (from *Brassica rapa*) and cyclohexane (anhydrous, 99.5%) were obtained from Sigma-Aldrich. Silicone oil (AP1000) was provided by Wacker Chemie AG. Deinonized water (resistivity > 18 MΩ cm) was produced from a Millipore Filter water system. All chemicals and solvents used in this study were commercially available and used as received unless stated otherwise.

### 2.2. Microfluidic chip

A T-shaped microfluidic device was used for generating monodispersed microcapsules with controllable sizes, see details in our previous work [11]. Briefly, the main chamber of the microfluidic chip was manufactured via a 3D printing (Formlabs Inc, Form 1+) using hydrophobic resin (Clear, FLGPCL03, Formlabs) for water-in-oil droplets generation. The production rate and microcapsule size were controlled by regulating the flow rates of the continuous and dispersed phases via a precised pressure pump (MFCS-EZ, Fluigent).

## 2.3. Assembly of microcapsule membrane

The assembly of microcapsule membrane was achieved by interfacial complexation of a positively charged polyelectrolyte (chitosan) with an oppositely charged surfactant (PFacid) at the water-in-oil droplet interface [11, 31, 46] (Fig. S1 in SI). First, a concentrated stock solution of chitosan (1% w/w) was prepared by dissolving the chitosan powder in deionized water over a night. The pH value of the solution ($\approx 3.0$) was adjusted by slowly adding hydrochloric acid. Undissolved impurities were then removed by syringe filters (poresize 5 $\mu$m, Sartorius Minisart). When used, the stock solution was diluted into 0.3 % w/w with deionized water and glycerol (pH value remains 3.0) as the dispersed phase. The oil phase (continuous phase) was prepared by dissolving PFacid in rapeseed oil at desired concentrations. Undissolved impurities were removed via centrifugation at 1000xG (Biofuge stratos, Heraeus) for 15 minutes. Water-in-oil droplets templates were subsequently produced by the microfluidic chip with low concentration (0.05 % w/w) of PFacid in the oil phase to pre-stabilize template interface reducing coalescence. The templates were collected for a short period of time with rapeseed oil, followed by transferring into a higher concentration of PFacid solution where the membrane is rapidly formed via interfacial complexation. The mechanical properties [11, 47] of these microcapsules were tuned by controlling the complexation time and concentration of PFacid. Finally, the microcapsules were washed thoroughly with a large volume of cyclohexane before being injected into the suspending fluid (WACKER® AP1000 silicone oil). The size standard deviation of microcapsules produced in our experiment is less than 2%. The size of the used capsules ranges from 40 to 90 $\mu$m in radius.

## 2.4. Membrane labeling

A commercially available fluorescent dye, Hostasol Yellow 3G (HY-3G) (from Clariant) was used to label microcapsule membrane. The dye was added in the oil phase during the membrane assembly and was absorbed onto the membrane. Excess dye was further removed with cyclohexane.

## 2.5. Atomic force microscopy (AFM)

The topography of microcapsule membrane was obtained by the AFM (Bioscope II, Bruker). The measurements were conducted using a silicone probe (spring constant 0.2 N/m, a tip radius 10 nm, NCLA-A, Bruker) in the tapping mode. The data were then processed and analysed using Gwyddion software. Prior to the measurement, microcapsules were dried on glass substrates at room temperature for a week in order to remove the internal fluid and surrounding cyclohexane.

## 2.6. Planar extensional flow

Microcapsules were deformed individually by a planar extensional flow generated in a cross-slot chamber [11, 34, 35]. The prepared microcapsule suspension was injected into the flow chamber with a glass syringe (FORTUNA) driven by an actuator (L-239.50SD, Physik Instrumente, Germany). A stepper motor controller (module C663, Mercury) was used to control the flow rate. The deformation of microcapsule was then visualized with an inverted microscope (Olympus IX-71) equipped with a high speed video camera (Photron Fastcam SA3). The visualisation was performed in two orthogonal planes (Fig. 1a).

In central area of the flow chamber, the velocity is determined as $[v_x, v_y, v_z] = [\dot{\epsilon}\mathrm{x}, -\dot{\epsilon}\mathrm{y}, 0]$, where $\dot{\epsilon}$ is the extensional rate. Particle Tracking Velocimetry (PTV) [48] was used to measure the velocity field at different $z$ positions and different flow rates, see details in our previous work [34].

In the vicinity of the flow stagnation point (SP), an initially spherical microcapsule was stretched in the elongational direction into an ellipsoid with a major and minor axis lengths $L$ and $S$, respectively (inset of Fig. 1b). The deformation was thus defined by the Taylor parameter [49], $D = (L-S)/(L+S)$. The viscous stress exerting on the membrane was balanced by its shear elasticity for the stationary deformation. In the regime of low Reynolds number (here, $Re < 0.01$), an asymptotic expression was derived [50],

$$D_\infty = \frac{5}{2}\frac{2+\nu_s}{1+\nu_s}\frac{\sigma R}{G_s}, \tag{1}$$

where $R$ is the radius of the undeformed microcapsule, $\sigma = \eta\dot{\epsilon}$ is viscous stress ($\eta$ is external fluid viscosity) and $G_s$ is surface shear elastic modulus. Here, the membrane thickness is much smaller than capsule radius, thus only surface modulus and Poisson's ratio $\nu_s$ are considered. We assume that $\nu_s$ is equal to 0.5 for incompressible material. This equation has been validated numerically and experimentally for small deformation [34, 51]. In the linear regime, the

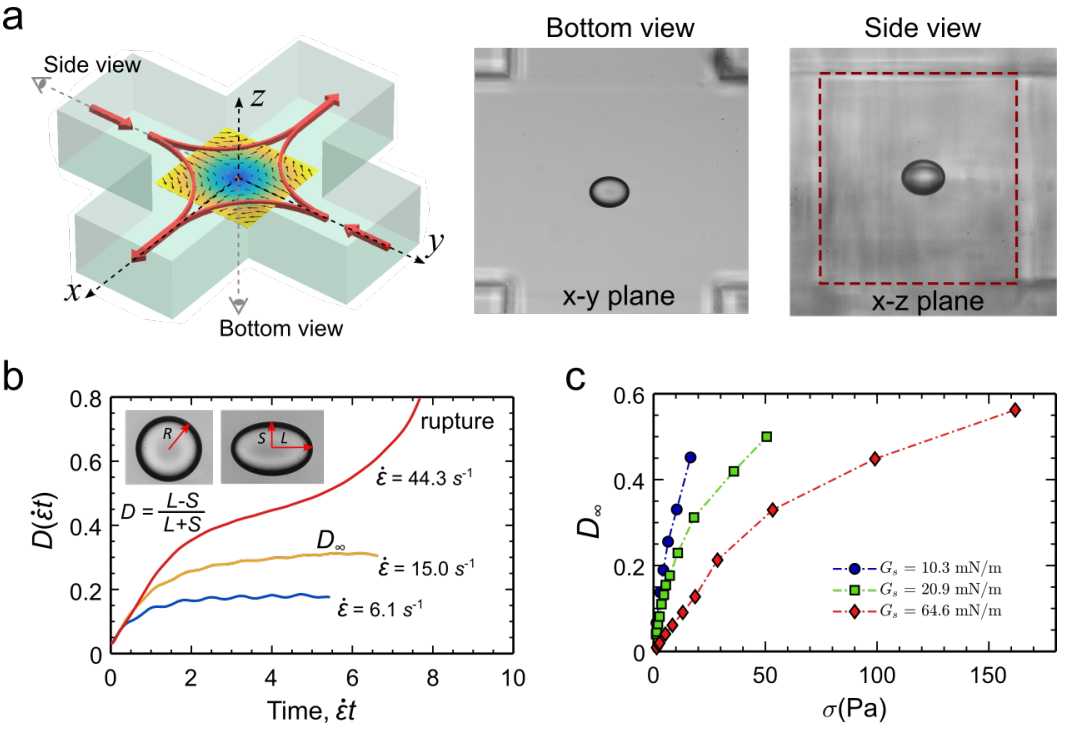


**Figure 1: Microcapsule deformation in the planar extensional flow. (a)** Visualization of capsule deformation in two views. High speed imaging shows the steady-state deformation of capsules in bottom view ($x$-$y$ plane) and side view ($x$-$z$ plane). Dashed frame indicates the walls of the 1 mm x 1 mm chamber. **(b)** Deformation of a capsule passing through the stagnation point of the extensional chamber as a function of dimensionless time $\dot{\varepsilon}t$. **(c)** Steady-state deformation as a function of the viscous stress for microcapsules with different shear moduli.

membrane shear elasticity $G_s$ can be estimated by deforming the microcapsule in different extensional rates. In the nonlinear regime, breakup of microcapsule was introduced when the flow strength was high enough.

### 2.7. Numerical modeling

To gain insight in the breakup of microcapsules, an essential feature is the internal stresses experienced by the membrane, namely the Cauchy elastic tensions. They are determined by a house-made numerical code. The system is a capsule filled and immersed in viscous Newtonian liquids which may be of different kinds. As the Reynolds number is much less than one, inertia is negligible. Stokes equations permit to calculate the velocity field by the implementation of the boundary-element method [52]. Our numerical modeling performs a coupling of finite-element-method to boundary-element method associated with Loop elements to describe the shape of the soft object [53]. It has been validated in different configurations namely droplets [54], vesicles [55] and other capsules [35, 53]. The results presented were obtained using the generalized Hooke's material law [56]. They are not qualitatively modified considering the neo-Hookean material law. The configurations are a capsule in a planar elongational flow and in a shear flow. The stationary shape and the two principal tensions are calculated. They are the tangential forces per unit length on the edges of a membrane patch in both directions. In the context of breakup, only the largest one (called $T_1$) is relevant.

## 3. Results and discussions

### 3.1. Observation of breakup

A microcapsule, having a spherical reference shape, is deformed rapidly when being exposed to the extensional flow (Fig.1b). It reaches a steady-state deformation $D_\infty$ when the viscous stresses are balanced by the membrane tension. The value of the steady-state deformation depends on the applied extensional rate $\dot{\varepsilon}$ for a given microcapsule (larger $\dot{\varepsilon}$ gives rise to a larger value of $D_\infty$ (Fig.1b)) and is found monotonically increasing with the viscous stress $\sigma$ (Fig.1c).

This relation is generally complex and depends on material properties, notably the shear elastic modulus. Breakup is observed when the steady-state deformation does not exist anymore (Fig.1b, $\dot{\epsilon} = 44.3\ s^{-1}$ for example). The critical rupture is defined as the first observation of membrane damage under a critical viscous stress $\sigma_{cr}$, an observation which is confirmed by a divergence of the Taylor parameter( Fig.1b, $\dot{\epsilon} = 44.3\ s^{-1}$).

## 3.2. Membrane properties

Firstly, the membrane properties are investigated statically using the pendant drop method. As shown in Fig.2, the presence of polyeclectrolyte (chitosan) and anionic surfactant strongly decreases the surface tension, approximately ten times. The time to reach equilibrium is typically 1-3 min and decreases with the concentration of surfactant. The final value of the tension, approximately 1-2 mN/m depends weakly on this concentration.

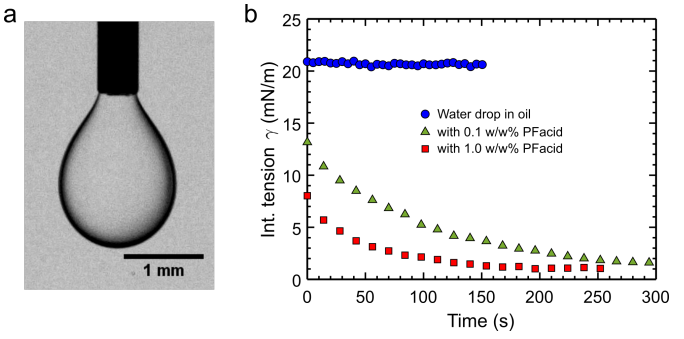


Figure 2: **Probing the interface properties via pendant drop for different drop/suspending fluid systems. (a)** A picture of an aqueous drop suspended in the oil phase by a needle. **(b)** The interfacial tension $\gamma$ vs. time for different testing systems. The tension dramatically decreases with time in the presence of the surfactant.

Secondly, the membrane properties are investigated by stressing the interface with the planar extensional flow. Within the limit of small deformations (up to $\approx 10\%$ for $D_\infty$ in our case), the relationship between the deformation and the viscous stress can be justifiably considered as linear [11]. For each microcapsule, various flow stresses $\sigma$ are applied and the stationary deformations $D_\infty$ are measured accordingly. In the limits of small deformations (linear regime, see Equation 1), we derive the shear elastic modulus $G_s$. The shear modulus $G_s$ is characterized by a rapid increment (almost two orders of magnitude) in the values of the apparent shear elastic modulus $G_s$ from 1 to 3 minutes of complexation as shown in Fig.3a. The term apparent $G_s$ is used here due to the complexity of separating in the first minute the surface tension from the elastic modulus. The values at times shorter than 1 minute are in agreement with the values of the surface tension. At larger complexation times, the membrane is clearly dominated by elasticity but the curve presents two kinds of elastic responses. This dual mechanical behavior is coherent with our recent work [39]. Indeed, it has been demonstrated that Chitosan/PFacid membrane is formed through the nucleation and further percolation of patch-like structures on the water-oil interface. Interface complexation time or the concentration of PFacid (concentration of chitosan is fixed in this work) predominately determines the state of the membrane. In the intermediate regime, the solid patches grow fast and pave the interface which is macroscopically characterized by a sudden increase of surface shear modulus. Surface elasticity also governs the membrane response (study in the linear regime of deformation). Once the interface is fully covered by the solid membrane, the membrane growth is governed by a diffusion limited process. The shear elastic modulus increases much weaker. Microscopically, the membrane topology probed with AFM reflects this process (Fig.3b-d). It indicates qualitative transition in the membrane mechanical properties during the complexation. See also supplementary information in Ref. [39]. Based on these measurements, we can infer the behaviour in the regime of large deformations. Indeed, we expect that the elastic network to be fragile in the intermediate regime and could present a solid-like to a liquid-like transition.

For simplicity, in the following we separate the investigated microcapsules into two categories: soft if $G_s$ lower than 50 mN/m and stiff where $G_s$ over 75 mN/m. Interestingly, wrinkling is only observed in the case of capsules with an elastic response: see Fig.S3 in SI.

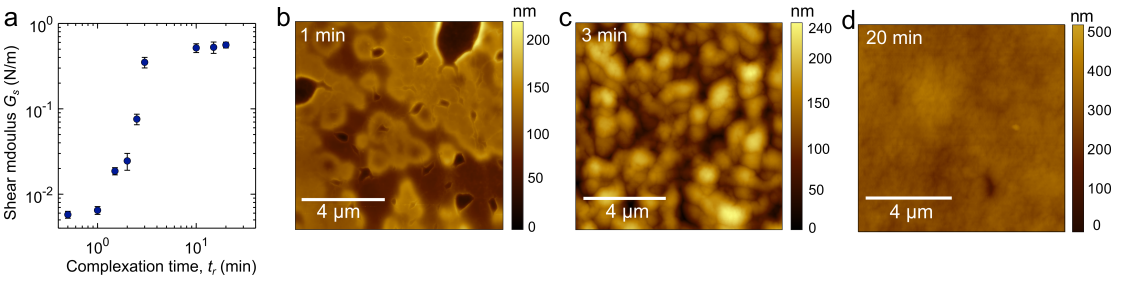


Figure 3: **Interface properties. (a)** Shear elastic modulus versus the complexation time of capsule membrane. **(b)-(d)** Surface topography of capsules membranes corresponding to different complexation times. Color bars indicate the thickness of the membranes.

### 3.3. Breakup of soft microcapsule

In general, the soft microcapsules demonstrate notable similarities in their behaviour with droplets specifically the axisymmetric nature of the stretching along the elongational direction. Additionally we can draw a parallel in breakup modes observed for soft microcapsules and reported for droplets in other studies [57–59]. In particular, wave instabilities such as Rayleigh-Plateau [59–62] are the most frequently observed mechanisms leading to breakup. The discussion of the large variety of modes observed for the soft microcapsule breakup will not be the focus of the current work. However, we will briefly introduce two most common scenarios observed in this system. The first case is observed when the imposed viscous stress is close to the critical breakup value (Fig.4). A soft microcapsule is gradually deformed into an ellipsoidal shape after being exposed in flow. A thinning waist appears afterwards in the midsection of the microcapsule. This shape is unstable and further two lobes are formed, similar to a dumbbell as observed in breakup of viscoelastic droplets in Newtonian fluids[63]. The waist is stretched thinner and thinner while the lobes keep the similar shape. Breakup eventually occurs by fragmenting the waist [11] (see Video S1). By visualising the breakup of soft capsules in two orthogonal planes we can confirm it being nearly axisymmetric as was mentioned above.

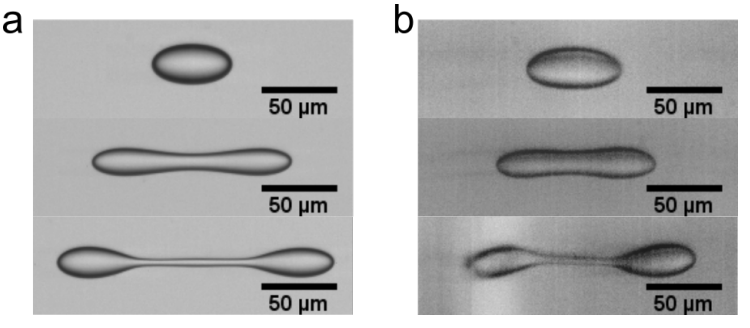


Figure 4: **Close-to-critical breakup of soft capsules in the extensional flow visualized in two orthogonal planes. (a)** Bottom view, the extensional rate is $\dot{\epsilon} = 67\ \mathrm{s}^{-1}$. **(b)** Side view, the extensional rate is $\dot{\epsilon} = 82\ \mathrm{s}^{-1}$. Shear elastic modulus of capsule is $G_s \approx 25$ mN/m.

The second mode of breakup is observed when the microcapsule is exposed to the viscous stress much larger than the critical one (Fig.5). In the early stage, similarly to the previous case, the microcapsule is deformed rapidly into an ellipsoidal shape. Afterwards, the microcapsule is stretched into a long cylinder-like shape, characterized by an approximately uniform thinning, to the point of eventual breakup into multiple secondary microcapsules.

Finally, the analysis of membrane properties at short times of complexation and the dynamics of capsule's shape lead to conclude that these modes of rupture are similar to fluid systems. This justifies to use breakup to name this regime.

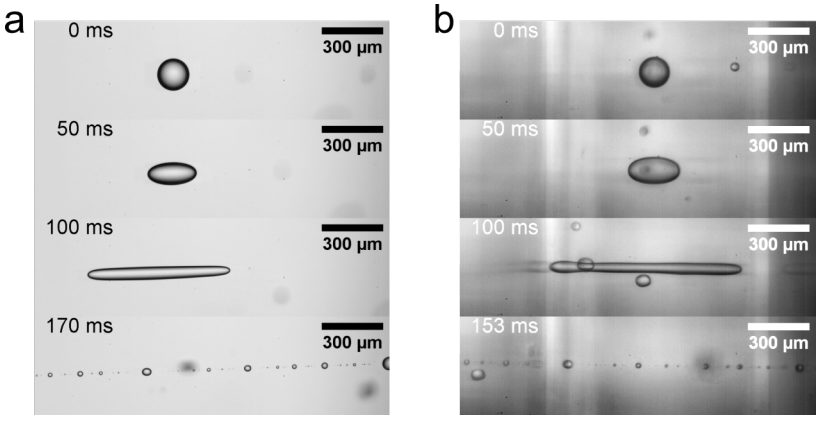


Figure 5: **Far-from-critical breakup of soft capsule in the extensional flow visualized in two orthogonal planes. (a)** Bottom view, the extensional rate is $\dot{\epsilon} = 58\,\mathrm{s}^{-1}$. **(b)** Side view, the extensional rate is $\dot{\epsilon} = 58\,\mathrm{s}^{-1}$. Shear elastic modulus of capsule is $G_s \approx 28$ mN/m.

### 3.4. Breakup of stiff microcapsule

Contrary to the case of soft capsule, after being deformed into an ellipsoid the stiff capsule doesn't show transition into a cylinder nor is it showing a thinning waist. A dark spot emerges on the membrane in the middle (highlighted by the red rectangles in Fig.6a), while on the bottom view the overall shape of capsule remains intact. However, on the side view (Fig. 6b) the dark spot corresponds to the onset of the membrane rupture. Our findings here illustrate that a conventionally single view is insufficient to correctly define capsule damage in flow. Complementary observations are thus necessary.

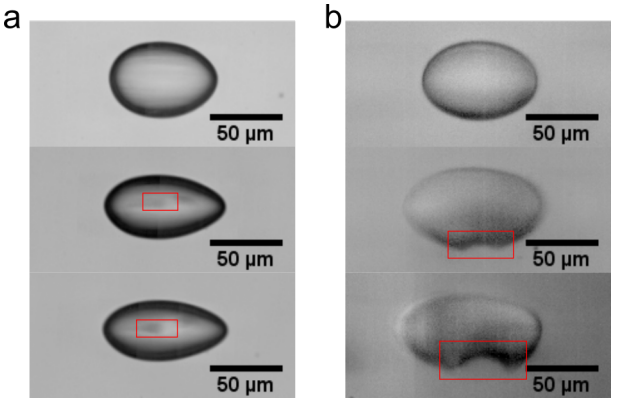


Figure 6: **Breakup onset of stiff capsule in the extensional flow visualized in two orthogonal planes. (a)** Bottom view, the extensional rate is $\dot{\epsilon} = 115\,\mathrm{s}^{-1}$. **(b)** Side view. the extensional rate is $\dot{\epsilon} = 433\,\mathrm{s}^{-1}$. Shear elastic modulus of capsules is $G_s \approx 94$ mN/m. Red rectangles indicate the local rupture of the membrane.

Fig. 7 shows an example of stiff capsule ($G_s \approx 138$ mN/m) breakup process visualized in two planes. The capsule is stretched along elongational direction while being simultaneously flattened in the x-z plane (Fig.7b). The overall shape is similar to a pancake which has been reported on HSA capsules in large deformation [35]. In further stretching, this asymmetry becomes more pronounced (20-28 ms Fig.7). Cusp tips appear on capsule, which can be observed on the bottom view (Fig.7a), while the rims are in general still intact and round on the side view (Fig.7b). The capsule eventually is broken with rough undulations on the surface (Fig.7b).

Such a rupture of elastic microcapsule was possible to observe thanks to our visualisation setup and to our knowledge it has not been reported yet. It is characterized by a first failure localized at the extremities of the minor axis of symmetry, which is normal to the elongational plane, while the shape remains smooth in the classical viewing plane (bottom view). On longest time, the difference between the two views becomes even more striking.

The interpretation needs additional information as a simple reasoning might have suggested that the capsule would break at the tips where the curvature is greatest. Indeed, it is the case of HSA capsules in shear flow [37] and the case of spinning polysiloxane capsules [64]. We will explain further this discrepancy. To gain insight, we assume that the constitutive law is still elastic and obeys a Hooke model. The following results are also valid with other laws. The Fig.8 presents the two principal tensions at the membrane $T_1$ (Fig.8a,c) and $T_2$ (Fig.8b,d) with $T_1 > T_2$. They refer to the membrane internal constraints. In the regime of large deformation, both tensions are positive meaning that all the membrane is stretched. The maximum value of $T_2$ over the capsule is approximately the minimum value of $T_1$. The maximal tension $T_1$ is localized at the point where rupture appears. In Fig.8e, a sketch allows to simply visualize how the surface forces per unit length, namely tensions are applied to a piece of membrane at the point of rupture. This outcome also corresponds to the spinning polysiloxane capsule [64]. The advantage of extensional flow and spinning is to avoid any fatigue phenomena as in shear flow [36, 37] where the membrane rotates and experiences successive dilatation, compression and also strong tip bending. Also, note that the rupture in shear flow is much more influenced by the presence of membrane defects and impurities which tank-tread around the vorticity axis perturbing the integrity of membrane. When exposed to the near threshold flow, the capsule undergoes relatively small deformation and rupture with only one notch occurrence in the middle part. However, in the far from threshold flow the capsule is rapidly stretched into a large deformation, several ruptures appear along the capsule (Figs S4,S5 in SI). Fluorescent image sequences (Fig.S6 in SI) confirm the discontinuous membrane happening at rupture for the large deformation. At beginning, the capsule remained spherical with inhomogeneous membrane (different labeling intensity). As the flow applied, it started to deform up to breakup, during which some locations on the membrane were not detected while some others were brighter. We believe that the area without fluorescence would be only water-oil interface while the fluorescent parts are the membrane fragments.

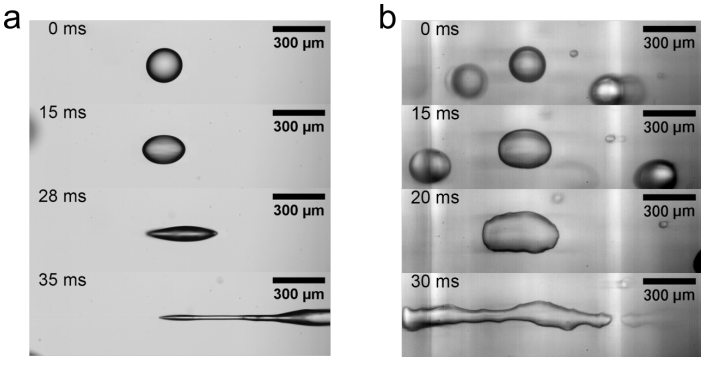


Figure 7: **Breakup of stiff capsule in the extensional flow visualized in two orthogonal planes. (a)** Bottom view, the extensional rate is $\dot{\varepsilon} = 1257\ \mathrm{s}^{-1}$. **(b)** Side view, the extensional rate is $\dot{\varepsilon} = 1446\,\mathrm{s}^{-1}$. The shear elastic modulus of capsules is about $G_s \approx 138$ mN/m.

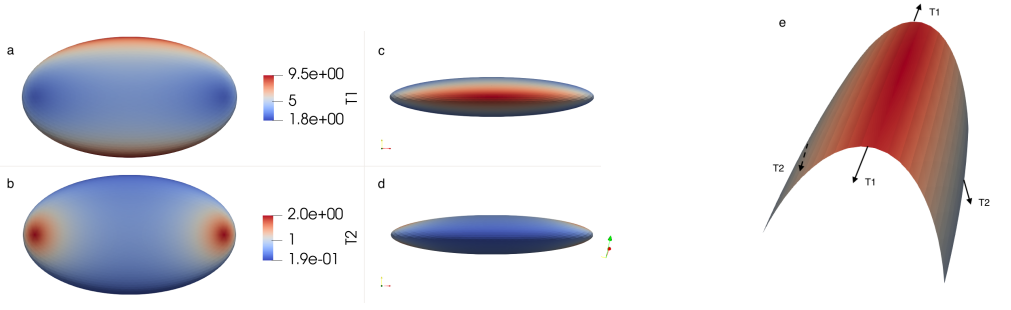


Figure 8: **Mechanical membrane tensions (internal constraints) over a capsule in planar extensional flow in two views**: **(a,b)** x-y plane, **(c,d)** x-z plane and **(e)** zoom with tensions where $T_1$ is maximum. The mechanical constitutive law is a Hooke model. The capillary number is $Ca = 1$. The maximum tension occurs in the central area at the bottom and the top of the capsule as expected to explain rupture. Tensions are scaled by the shear elastic modulus.

### 3.5. Post breakup analysis

In this section we investigate the state of the daughter capsules after the breakup. Capsules of both categories - soft and stiff - with fluorescently labeled membranes were burst and the products of their breakup were pulled back to the field of view for characterisation and analysis. Fig. 9 illustrates two typical post breakup cases of capsules with different membrane shear elasticity. When the membrane is broken, the core liquid spills out. That drastically increases the surface-to-volume ratio causing the shortage of membrane material to cover all the water-oil interface even if assuming an overall reorganization. The shapes of the daughter capsules are found to qualitatively depend on the membrane stiffness. In Fig. 9a, all the daughter capsules remain spherical for the soft parent capsule after breakup. In contrast, irregular shapes are observed on daughter capsules of the stiff parent capsule (Fig.9b, also in SI).

We find that almost all secondary capsules derived from soft parent capsules exhibit fluorescence even though not uniformly (Fig.9a2). Combined with nearly spherical shape of all the secondary capsules this indicates the capacity of the membrane material to form a new interface driven by surface tension and shows its fluid properties similarly to surfactant-laden droplets [65]. Interfacial tension drives the formation of daughter capsules by minimizing surface energy, similar to liquid-liquid droplet breakup in flow [58]. This is consistent with our observation of capsule membrane composed with liquid and solid patches in short complexation time [39].

Fig. 9b shows the post breakup state of a rigid parent capsule. It's characterized by two big noticeably non-spherical fragments that emit heterogeneous fluorescent signal and smaller several spherical fragments that do not show any fluorescence. It indicates the lack of membrane material to cover the increased cumulative area of the interface. This observation additionally supports the qualitative differences between two categories of capsules.

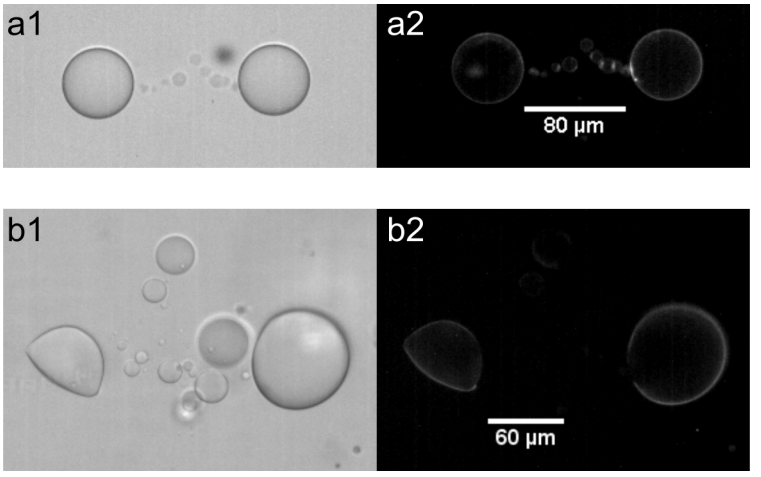


Figure 9: **Two distinct post breakup cases for capsules with different membrane stiffness. (a)** Soft capsule with $G_s \approx 0.012$ N/m. **(b)** Rigid capsule with $G_s \approx 0.2$ N/m. The images in the left and right columns are the bright and fluorescent fields, respectively.

### 3.6. Phase diagram of breakup

Two modes of breakup have been previously identified. They are linked to the nature of the mechanical response of the membrane: liquid-like or solid-like. Here, we report a detailed investigation in the space of parameters ($G_s, \sigma R$), namely the shear elastic modulus versus the applied hydrodynamic tension (the force per unit length) (Fig. 10). Larger capsules exposed to the same hydrodynamic stress experience larger deformations, however neither effective $G_s$ nor critical stress $\sigma_c R$ depend on the capsule size ( See SI Fig. 8). Below a critical stress $\sigma_c R$, the capsule never breaks whatever the mode. In the limit of small shear elastic modulus (the liquid-like behavior), this stress $\sigma_c R \approx 40$ mN/m depends weakly on $G_s$ leading to a capillary number about 0.2, a consistent value with the Grace curve [66]. As expected, the critical stress increases monotonously when the membrane is dominated by the elastic response. This transition occurs at shear modulus $G_s$ roughly between 40 mN/m and 70 mN/m which corresponds to the liquid-like to solid-like transition characterized by a strong increase of the effective elastic modulus (Fig.3a). This transition also marks the behavior at higher hydrodynamic stress. Indeed, whatever a smaller shear elastic modulus, the rupture leads to a drop-like fragmentation, dumbell (near threshold) or waist (far from threshold). Above this shear elastic modulus,

the shape is more irregular leading to a lack of membrane continuity, an observation confirmed by the visualization of the membrane by fluorescence (Fig.S6 in SI). It corresponds to the breakup of an elastic capsule as studied previously.

In the reference [10], the authors studied the dynamics of particle-covered droplets in shear flow and found the the breakup patterns morphologically similar to those we observed for low $G_s$ capsules. At a high surface coverage, the nano-particle laden interface undergoes a transition from a liquid to an elastic shell. The addition of surface active agents drastically changes the rheological properties of the droplet interface. With an increasing concentration of the interfacially active compounds the droplet interface may obtain a solid-like behaviour. However, separating the thermodynamic and a viscoelastic contributions is a challenging task [67]. We observe a similar phenomenon if we consider that at short complexation times the chitosan/PFacid interface is only partially covered by small patches of solid matter as we showed in our previous work [39] and in our AFM measurements (Fig. 3 b-d). The mobility of the patches at the interface explains its pronounced fluidity. Thus drop-like breakup modes of capsules at low apparent $G_s$ and $\sigma R$ independency of $G_s$ are explained by the dominant role of interfacial tension.

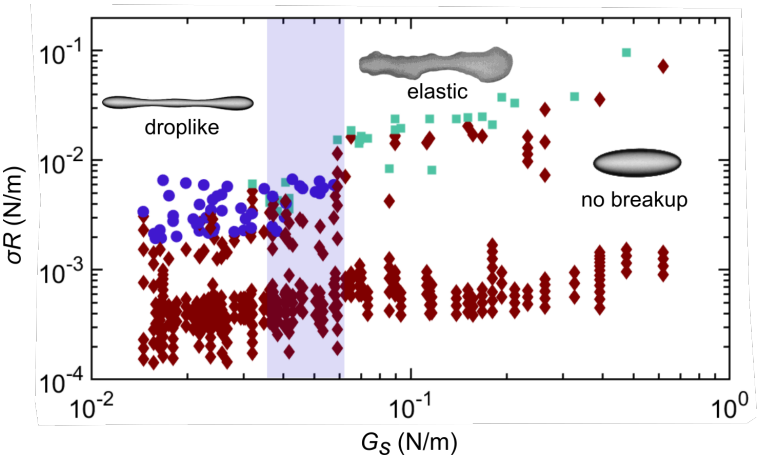


Figure 10: **Phase diagram of capsule breakup in $\sigma R$-$G_s$ parameter space.** The symbols ◇, ○ and □ denote no breakup, drop-like behavior (breakup) and elastic behavior of capsules (solid-like breakup also called breakage), respectively. The diameter of used capsules ranges from 80 to 180 $\mu$m. The shaded region indicates the transition zone between drop-like and elastic behaviors breakup. Inset images are typical shapes observed.

## 4. Conclusion

The present work shows the systematic experimental study of the rupture of weakly cohesive microcapsules resulting from interfacial polycondensation. The study is performed in a planar extensional flow, a configuration providing a benefit of simpler capsule dynamics, i.e. no membrane tank-treading, and consequently no fatigue failure of the capsule and the presence of stagnation point to fix the field of view. Additionally, our setup allows for the observation of the capsule in two orthogonal planes of view which provides an opportunity to accurately examine the integrity of the capsule in flow.

The microcapsule undergoes linear and non-linear deformation prior to breakup with a viscoplastic response shown when it is relaxed without any rupture [11]. The shear elastic modulus of individual capsules is measured in the regime of small deformations. Consequently each capsule is subjected to large deformations up to the point of membrane rupture. The modes of rupture are closely related to the membrane mechanical properties and to the shell structure. Capsules with low apparent membrane shear elasticity manifest drop-like rupture. Continuous thinning of the membrane in deformation prompts the membrane destabilization where it is most likely the membrane shows a transition from a solid to liquid state. While solid-like rupture (breakage) with a discontinuity of the membrane occurs for the capsule with high shear elasticity. The maximal internal constraint (maximal membrane tension) marks the point of rupture emergence.

The results presented in this work demonstrate the rich dynamics of the capsule rupture in the extensional flow allowing to expect the behavior in shear flow based on the numerical calculation of mechanical tensions (Fig.S7 in SI). At low complexation times, the chitosan capsule is expected to exhibit a characteristic S-shape [37, 68] with the

tips emitting small capsules. At large complexation times and moderate shear rate, the chitosan capsule is expected to break along the axis of vorticity where the membrane tension is maximal. Finally, the results may provide the basic principles for the design of targeted drug carriers and release of encapsulated materials.

## Conflicts of interest

The authors declare that they have no known competing financial interests or personal relationships that could have appeared to influence the work reported in this paper.

## Credit author statement

**Revaz Chachanidze and Kaili Xie** (equal contributions): experimental investigations, analysis of data, methodology, writing - original draft, review and editing. **Jinming Lyu**: numerical investigations. **Marc Jaeger**: conceptualization, supervision. **Marc Leonetti**: conceptualization, methodology, original draft, supervision.

## Acknowledgements

Centre de Calcul Intensif d'Aix-Marseille is acknowledged for granting access to their high-performance computing resources. The authors thank CNES (Centre National d'Etudes Spatiales) and ANR (ANR-18-CE06-0008) for financial support. The authors thank D. Barthes-Biesel, P. G. Chen, J. Deschamps, J. Gubspun, G. Boedec, C. de Loubens, M. Georgelin and A-V. Salsac for helpful discussions. K. Xie also thanks Fabien MOROTE for the help of AFM measurement.

## References

[1] C. H. Peterson, S. S. Anderson, G. N. Cherr, R. F. Ambrose, S. Anghera, S. Bay, M. Blum, R. Condon, T. A. Dean, M. Graham, et al., A tale of two spills: novel science and policy implications of an emerging new oil spill model, BioScience 62 (5) (2012) 461–469.

[2] R. Clift, J. R. Grace, M. E. Weber, Bubbles, drops, and particles (2005).

[3] R. I. Dekker, A. Deblais, K. P. Velikov, P. Veenstra, A. Colin, H. Kellay, W. K. Kegel, D. Bonn, Emulsion destabilization by squeeze flow, Langmuir 36 (27) (2020) 7795–7800.

[4] L. Champougny, M. Roché, W. Drenckhan, E. Rio, Life and death of not so "bare" bubbles, Soft Matter 12 (24) (2016) 5276–5284.

[5] E. Rideau, R. Dimova, P. Schwille, F. R. Wurm, K. Landfester, Liposomes and polymersomes: a comparative review towards cell mimicking, Chemical society reviews 47 (23) (2018) 8572–8610.

[6] M. Dionzou, A. Morère, C. Roux, B. Lonetti, J.-D. Marty, C. Mingotaud, P. Joseph, D. Goudounèche, B. Payré, M. Léonetti, et al., Comparison of methods for the fabrication and the characterization of polymer self-assemblies: what are the important parameters?, Soft matter 12 (7) (2016) 2166–2176.

[7] D. J. McClements, Protein-stabilized emulsions, Current opinion in colloid & interface science 9 (5) (2004) 305–313.

[8] A. Stocco, E. Rio, B. P. Binks, D. Langevin, Aqueous foams stabilized solely by particles, Soft Matter 7 (4) (2011) 1260–1267.

[9] C. Monteux, J. Kirkwood, H. Xu, E. Jung, G. G. Fuller, Determining the mechanical response of particle-laden fluid interfaces using surface pressure isotherms and bulk pressure measurements of droplets, Physical chemistry chemical physics 9 (48) (2007) 6344–6350.

[10] Y. Mei, G. Li, P. Moldenaers, R. Cardinaels, Dynamics of particle-covered droplets in shear flow: unusual breakup and deformation hysteresis, Soft Matter 12 (47) (2016) 9407–9412.

[11] K. Xie, C. de Loubens, F. Dubreuil, D. Z. Gunes, M. Jaeger, M. Leonetti, Interfacial rheological properties of self-assembling biopolymer microcapsules, Soft Matter 13 (36) (2017) 6208–6217.

[12] D. Kumar, J. D. Paulsen, T. P. Russell, N. Menon, Wrapping with a splash: High-speed encapsulation with ultrathin sheets, Science 359 (6377) (2018) 775–778.

[13] F. Sicard, J. Toro-Mendoza, A. Striolo, Nanoparticles actively fragment armored droplets, ACS nano 13 (8) (2019) 9498–9503.

[14] M. Kaganyuk, A. Mohraz, Shear-induced deformation and interfacial jamming of solid-stabilized droplets, Soft matter 16 (18) (2020) 4431–4443.

[15] L. C. Corrêa-Filho, M. Moldão-Martins, V. D. Alves, Advances in the application of microcapsules as carriers of functional compounds for food products, Applied Sciences 9 (3) (2019) 571.

[16] E. Assadpour, S. M. Jafari, Advances in spray-drying encapsulation of food bioactive ingredients: From microcapsules to nanocapsules, Annual review of food science and technology 10 (2019) 103–131.

[17] L. Kromidas, E. Perrier, J. Flanagan, R. Rivero, I. Bonnet, Release of antimicrobial actives from microcapsules by the action of axillary bacteria, International journal of cosmetic science 28 (2) (2006) 103–108.

[18] H. Huang, Y. Yu, Y. Hu, X. He, O. Berk Usta, M. L. Yarmush, Generation and manipulation of hydrogel microcapsules by droplet-based microfluidics for mammalian cell culture, Lab Chip 17 (11) (2017) 1913–1932.

[19] C. Perignon, G. Ongmayeb, R. J. Neufeld, Y. A. Frere, D. Poncelet, Microencapsulation by interfacial polymerisation: membrane formation and structure, Journal of Microencapsulation 32 (2015) 1 – 15.

[20] A. Madene, M. Jacquot, J. Scher, S. Desobry, Flavour encapsulation and controlled release–a review, International journal of food science & technology 41 (1) (2006) 1–21.

[21] H.-S. Jeong, E. Kim, C. Nam, Y. Choi, Y.-J. Lee, D. A. Weitz, H. Lee, C.-H. Choi, Hydrogel microcapsules with a thin oil layer: Smart triggered release via diverse stimuli, Advanced Functional Materials 31 (18) (2021) 2009553.

[22] A. Abbaspourrad, S. S. Datta, D. A. Weitz, Controlling release from ph-responsive microcapsules, Langmuir 29 (41) (2013) 12697–702.

[23] L. Liu, J.-P. Yang, X.-J. Ju, R. Xie, Y.-M. Liu, W. Wang, J.-J. Zhang, C. H. Niu, L.-Y. Chu, Monodisperse core-shell chitosan microcapsules for ph-responsive burst release of hydrophobic drugs, Soft Matter 7 (10) (2011) 4821–4827.

[24] M. Ina, A. P. Zhushma, N. V. Lebedeva, M. Vatankhah-Varnoosfaderani, S. D. Olson, S. S. Sheiko, The design of wrinkled microcapsules for enhancement of release rate, Journal of colloid and interface science 478 (2016) 296–302.

[25] F. Huang, W.-C. Liao, Y. S. Sohn, R. Nechushtai, C.-H. Lu, I. Willner, Light-responsive and ph-responsive dna microcapsules for controlled release of loads, Journal of the American Chemical Society 138 (28) (2016) 8936–8945.

[26] Y. Xu, Y. Shen, T. C. Michaels, D. Baumgallino2018edgeolo, Q. Peter, Y. Lu, K. L. Saar, D. Vella, H. Zhu, et al., Deformable and robust core-shell protein microcapsules templated by liquid-liquid phase-separated microdroplets, Advanced Materials Interfaces 8 (19) (2021) 2101071.

[27] A. Le Goff, B. Kaoui, G. Kurzawa, B. Haszon, A. V. Salsac, Squeezing bio-capsules into a constriction: deformation till break-up, Soft Matter 13 (41) (2017) 7644–7648.

[28] M. G. Bah, H. M. Bilal, J. Wang, Fabrication and application of complex microcapsules: A review, Soft Matter 16 (3) (2020) 570–590.

[29] W. Tong, X. Song, C. Gao, Layer-by-layer assembly of microcapsules and their biomedical applications, Chemical Society Reviews 41 (18) (2012) 6103–6124.

[30] C. S. Peyratout, L. Daehne, Tailor-made polyelectrolyte microcapsules: from multilayers to smart containers, Angewandte Chemie International Edition 43 (29) (2004) 3762–3783.

[31] D. Z. Gunes, M. Pouzot, M. Rouvet, S. Ulrich, R. Mezzenga, Tuneable thickness barriers for composite o/w and w/o capsules, films, and their decoration with particles, Soft Matter 7 (19) (2011) 9206–9215.

[32] I. Koleva, H. Rehage, Deformation and orientation dynamics of polysiloxane microcapsules in linear shear flow, Soft Matter 8 (13) (2012) 3681.

[33] T. X. Chu, A.-V. Salsac, E. Leclerc, D. Barthès-Biesel, H. Wurtz, F. Edwards-Lévy, Comparison between measurements of elasticity and free amino group content of ovalbumin microcapsule membranes: discrimination of the cross-linking degree, Journal of colloid and interface science 355 (1) (2011) 81–88.

[34] C. de Loubens, J. Deschamps, M. Georgelin, A. Charrier, F. Edwards-Levy, M. Leonetti, Mechanical characterization of cross-linked serum albumin microcapsules, Soft matter 10 (25) (2014) 4561–4568.

[35] C. de Loubens, J. Deschamps, G. Boedec, M. Leonetti, Stretching of capsules in an elongation flow, a route to constitutive law, Journal of Fluid Mechanics 767 (2015).

[36] K.-S. Chang, W. L. Olbricht, Experimental studies of the deformation and breakup of a synthetic capsule in steady and unsteady simple shear flow, Journal of Fluid Mechanics 250 (1993) 609–633.

[37] S. Joung, M. Song, D. Kim, Synthetic capsule breakup in simple shear flow, Physics of Fluids 32 (11) (2020) 113603.

[38] H. A. Stone, Dynamics of drop deformation and breakup in viscous fluids, Annual review of fluid mechanics 26 (1) (1994) 65–102.

[39] R. Chachanidze, K. Xie, H. Massaad, D. Roux, M. Leonetti, C. de Loubens, Structural characterization of the interfacial self-assembly of chitosan with oppositely charged surfactant, Journal of Colloid and Interface Science 616 (2022) 911–920.

[40] A. Yazdani, P. Bagchi, Influence of membrane viscosity on capsule dynamics in shear flow, Journal of Fluid Mechanics 718 (2013) 569–595.

[41] S. Kessler, R. Finken, U. Seifert, Swinging and tumbling of elastic capsules in shear flow, Journal of Fluid Mechanics 605 (10 2007).

[42] Y. Sui, H. Low, Y. Chew, P. Roy, Tank-treading, swinging, and tumbling of liquid-filled elastic capsules in shear flow, Physical Review E 77 (1) (2008) 016310.

[43] S. D. Hudson, J. T. Cabral, W. J. Goodrum Jr, K. L. Beers, E. J. Amis, Microfluidic interfacial tensiometry, Applied Physics Letters 87 (8) (2005) 081905.

[44] J. T. Cabral, S. D. Hudson, Microfluidic approach for rapid multicomponent interfacial tensiometry, Lab on a Chip 6 (3) (2006) 427–436.

[45] S. Haward, Microfluidic extensional rheometry using stagnation point flow, Biomicrofluidics 10 (4) (2016) 043401.

[46] M. Maleki, C. de Loubens, K. Xie, E. Talansier, H. Bodiguel, M. Leonetti, Membrane emulsification for the production of suspensions of uniform microcapsules with tunable mechanical properties, Chemical Engineering Science 237 (2021) 116567.

[47] C. Trégouët, T. Salez, C. Monteux, M. Reyssat, Transient deformation of a droplet near a microfluidic constriction: A quantitative analysis, Physical Review Fluids 3 (5) (2018) 053603.

[48] K.-W. Hsiao, J. Dinic, Y. Ren, V. Sharma, C. M. Schroeder, Passive non-linear microrheology for determining extensional viscosity, Physics of Fluids 29 (12) (2017) 121603.

[49] G. I. Taylor, The formation of emulsions in definable fields of flow, Proceedings of the Royal Society of London. Series A, containing papers of a mathematical and physical character 146 (858) (1934) 501–523.

[50] D. Barthès-Biesel, H. Sgaier, Role of membrane viscosity in the orientation and deformation of a spherical capsule suspended in shear flow, Journal of Fluid Mechanics 160 (1985) 119–135.

[51] E. Lac, D. BarthèS-Biesel, N. A. Pelekasis, J. Tsamopoulos, Spherical capsules in three-dimensional unbounded stokes flows: effect of the membrane constitutive law and onset of buckling, Journal of Fluid Mechanics 516 (2004).

[52] C. Pozrikidis, et al., Boundary integral and singularity methods for linearized viscous flow, Cambridge university press, 1992.

[53] G. Boedec, M. Leonetti, M. Jaeger, Isogeometric fem-bem simulations of drop, capsule and vesicle dynamics in stokes flow, J. Comp. Phys. 342 (2017) 117–138.

[54] J. Gounley, G. Boedec, M. Jaeger, M. Leonetti, Influence of surface viscosity on droplets in shear flow, Journal of Fluid Mechanics 791 (2016) 464–494.

[55] G. Boedec, M. Leonetti, M. Jaeger, 3d vesicle dynamics simulations with a linearly triangulated surface, J. Comp. Phys. 230 (2011) 1020–1034.

[56] C. Pozrikidis, Modeling and simulation of capsules and biological cells, Chapman and Hall/CRC, 2003.
[57] B. Bentley, L. G. Leal, An experimental investigation of drop deformation and breakup in steady, two-dimensional linear flows, Journal of Fluid Mechanics 167 (1986) 241–283.
[58] S. Kaur, L. G. Leal, Drop deformation and break-up in concentrated suspensions, Journal of Rheology 54 (5) (2010) 981–1008.
[59] E. Villermaux, Fragmentation, Annu. Rev. Fluid Mech. 39 (2007) 419–446.
[60] S. Tomotika, On the instability of a cylindrical thread of a viscous liquid surrounded by another viscous fluid, Proceedings of the Royal Society of London. Series A-Mathematical and Physical Sciences 150 (870) (1935) 322–337.
[61] A. Pandey, M. Kansal, M. A. Herrada, J. Eggers, J. H. Snoeijer, Elastic rayleigh–plateau instability: dynamical selection of nonlinear states, Soft matter 17 (20) (2021) 5148–5161.
[62] G. Boedec, M. Jaeger, M. Leonetti, Pearling instability of a cylindrical vesicle, Journal of fluid mechanics 743 (2014) 262–279.
[63] W. Milliken, L. Leal, Deformation and breakup of viscoelastic drops in planar extensional flows, Journal of non-newtonian fluid mechanics 40 (3) (1991) 355–379.
[64] M. Husmann, H. Rehage, E. Dhenin, D. Barthès-Biesel, Deformation and bursting of nonspherical polysiloxane microcapsules in a spinning-drop apparatus, Journal of colloid and interface science 282 (1) (2005) 109–119.
[65] G. Espinosa, I. Lopez-Montero, F. Monroy, D. Langevin, Shear rheology of lipid monolayers and insights on membrane fluidity, Proc Natl Acad Sci U S A 108 (15) (2011) 6008–13.
[66] H. P. Grace, Dispersion phenomena in high viscosity immiscible fluid systems and application of static mixers as dispersion devices in such systems, Chemical Engineering Communications 14 (3-6) (1982) 225–277.
[67] T. Verwijlen, L. Imperiali, J. Vermant, Separating viscoelastic and compressibility contributions in pressure-area isotherm measurements, Advances in colloid and interface science 206 (April 2014).
[68] C. de Loubens, J. Deschamps, F. Edwards-Levy, M. Leonetti, Tank-treading of microcapsules in shear flow, Journal of Fluid Mechanics 789 (2016) 750–767.